

A Bias-Free Training Paradigm for More General AI-generated Image Detection

Fabrizio Guillaro¹ Giada Zingarini¹ Ben Usman² Avneesh Sud²
 Davide Cozzolino¹ Luisa Verdoliva¹

¹University Federico II of Naples ²Google DeepMind

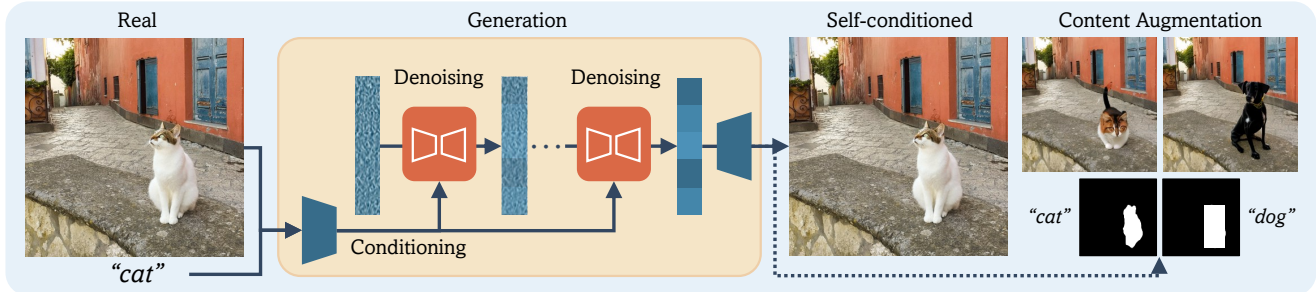


Figure 1. We introduce a new training paradigm for AI-generated image detection. To avoid possible biases, we generate synthetic images from self-conditioned reconstructions of real images and include augmentation in the form of inpainted versions. This allows to avoid semantic biases. As a consequence, we obtain better generalization to unseen models and better calibration than SoTA methods.

Abstract

Successful forensic detectors can produce excellent results in supervised learning benchmarks but struggle to transfer to real-world applications. We believe this limitation is largely due to inadequate training data quality. While most research focuses on developing new algorithms, less attention is given to training data selection, despite evidence that performance can be strongly impacted by spurious correlations such as content, format, or resolution. A well-designed forensic detector should detect generator specific artifacts rather than reflect data biases. To this end, we propose *B-Free*, a bias-free training paradigm, where fake images are generated from real ones using the conditioning procedure of stable diffusion models. This ensures semantic alignment between real and fake images, allowing any differences to stem solely from the subtle artifacts introduced by AI generation. Through content-based augmentation, we show significant improvements in both generalization and robustness over state-of-the-art detectors and more calibrated results across 27 different generative models, including recent releases, like *FLUX* and *Stable Diffusion 3.5*. Our findings emphasize the importance of a careful dataset curation, highlighting the need for further research in dataset design. Code and data will be publicly available at <https://grip-unina.github.io/B-Free/>.

1. Introduction

The rise of generative AI has revolutionized the creation of synthetic content, enabling easy creation of high-quality sophisticated context, even for individuals without deep technical expertise. Thanks to user-friendly interfaces and pre-trained models, users can create high-quality synthetic content such as text, images, music, and videos through simple inputs or prompts [50]. This accessibility has democratized content creation, enabling professionals in fields like design, marketing, and entertainment to leverage AI for creative purposes. However, this raises concerns about potential misuse, such as the creation of deepfakes, misinformation, and challenges related to intellectual property and content authenticity [4, 16, 25].

Key challenges for current GenAI image detectors include generalization — detecting synthetic generators not present in the training set — and ensuring robustness against image impairments caused by online sharing, such as compression, resizing, and cropping [41]. In this context, large pre-trained vision-language models like CLIP [34] have demonstrated impressive resilience to these distribution shifts [31]. The success of these models in forensic applications suggests that pre-training on large and diverse datasets may be a promising path forward. An important aspect often overlooked in the current literature is selection of good task specific datasets to train or fine-tune such models, that primarily rely on hidden, unknown signa-

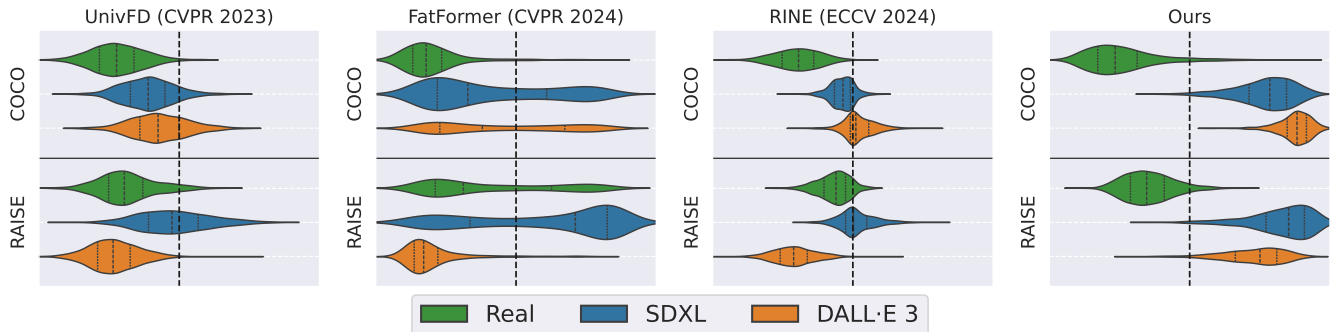


Figure 2. Forensic detectors can exhibit opposite behaviors depending on their training dataset. The four plots show the prediction distributions for three CLIP-based detectors, UnivFD [31], FatFormer [27] and RINE [21], and the proposed one. The fake images (SD-XL or DALL-E 3) are generated from images of a single dataset (RAISE on top, COCO on the bottom) and tested only against real images of the same dataset (Synthbuster [2] and the test dataset from [11]). We observe that for the same detector (e.g., RINE) and the same fake-image generator (e.g., DALL-E 3) the score distributions can vary significantly depending on the dataset used, going from real (left of the dotted line) to fake (right of the dotted line) or vice versa. This is likely due to the presence of biases in the training set that heavily impact the detector prediction. Our detector, on the other hand, shows consistent and correct results in all cases.

tures of generative models [30, 47]. Indeed, it is important to guarantee that the detector decisions are truly based on generation-specific artifacts and not on possible dataset biases [7, 28, 42]. In fact, datasets used during the training and testing phases of forensic classifiers could be affected by different types of polarization.

Format issues have been the Achilles’ heel of forensic detectors since at least 2013, when [5] recognized that a dataset for image tampering detection [13] included forged and pristine images compressed with different JPEG quality factors. Therefore, a classifier trained to discriminate tampered and pristine images may instead learn their different processing histories. This issue has been highlighted in [18] with reference to datasets of synthetic and real images. In fact, the former are often created in a lossless format (PNG), while the latter are typically compressed in lossy formats like JPEG. Again a classifier could learn coding inconsistencies instead of forensic clues. Likewise it could learn re-sampling artifacts, as it was recently shown in [35] - in this case a bias was introduced by resizing all the real images from the LAION dataset to same resolution, while keeping the fake ones unaltered.

Forensic clues are subtle and often imperceptible to the human eye, making it easy to introduce biases when constructing the training and test sets, as well as the evaluation protocol. Semantic content itself can also represent a source of bias. For this reason, several recent proposals [2, 3, 11] take great care to include pairs of real and fake images characterized by the same prompts when building a training or test dataset. To gain better insights about the above issues, in Fig. 2 we show the performance of three SoTA CLIP-based approaches [21, 27, 31] in distinguishing real images from fake images generated by SD-XL and DALL-E 3. For each method we consider two settings: in

the first case, real images come from the RAISE dataset [12] and fakes are generated starting from images of the same dataset. The second case uses COCO as source of reals instead of RAISE. FakeInversion [7] proposes an effective approach towards semantic alignment of training data using reverse image search to find matching reals, however fails to capture real image distribution after 2021.

To mitigate potential dataset biases, in this work we propose a new training paradigm, B-Free, where we generate synthetic images using self-conditioned reconstructions of real images and incorporate augmented, inpainted variations. This approach helps prevent semantic bias and potential misalignment in coding formats. The model analyzes the whole image during training to avoid unnecessary cropping or resizing operations, the latter being particularly harmful since it could wash out the subtle low-level forensic clues [17]. Overall, we make the following contributions:

- We propose a large curated training dataset of 51k real and 309k fake images. Real images are sourced from COCO, while synthetic images are self-conditioned reconstructions using Stable Diffusion 2.1. This helps the detector to focus on artifacts related to the synthetic generation process avoiding content and coding related biases.
- We show that including proper content-based augmentation provides better calibrated results. This ensures that in-lab performance is closer to expected performance on real-world images shared over social networks.
- We study the effect of different distribution shifts and show that by leveraging a pre-trained large model trained on our dataset, it is possible to obtain a SoTA accuracy (87%) even on unseen new generators.

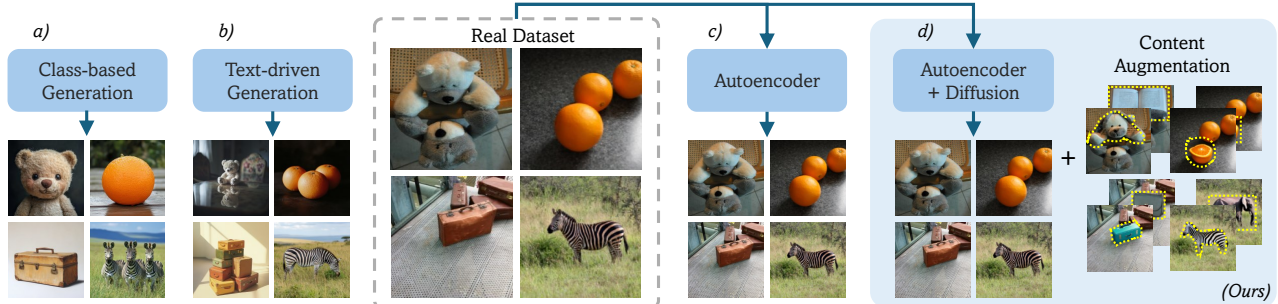


Figure 3. Overview of existing (a, b, c) and proposed (d) strategies for building an aligned training dataset. Some methods try to match synthetic images to the corresponding real images by using class-based generation (a) or text-to-image generation with real images’ descriptions (b). In (c) real images are fed to an autoencoder to generate a **reconstructed fake** with the same content. Unlike in (c), in our approach (d) a **self-conditioned fake** is generated using diffusion steps, and we also add a content augmentation step.

2. Related Work

A well-curated training set is of vital importance for any data-driven method. In recent years this awareness has much grown also in the forensic field and there have been many efforts in this direction following two main lines of work: *i)* forming a reliable dataset by carefully selecting “natural” fakes, or *ii)* creating a fully synthetic dataset by injecting forensic artifacts in real images.

Selecting good natural training data. Wang et al.’s paper [43] was among the first to demonstrate the importance of selecting a suitable training set for gaining generalization to unseen synthetic generators. The selected dataset included images from a single generation architecture (ProGAN) and 20 different real/false categories (Fig. 3.a) and included augmentation in the form of common image post-processing operations, such as blurring and compression. Results clearly show that generalization and robustness strongly benefit from the many different categories included during training as well as from the augmentation procedure. In fact, this dataset has been widely utilized in the literature, where researchers follow a standard protocol assuming the knowledge of one single generative model during training. This scenario describes a typical real world situation where new generative architectures are unknown at test time.

The dataset proposed in [43] was used in [31] to fine-tune a CLIP model with a single learnable linear layer, achieving excellent generalization not only on GAN models but also on Diffusion-based synthetic generators never seen during training. Likewise, it was used in [21] to train a CNN classifier that leverages features extracted from CLIP’s intermediate layers to better exploit low-level forensic features. In [37, 40] image captions (either paired to the dataset images or generated from them) were used as additional input for a joint analysis during training. The approach proposed in [27] is trained using only 4 classes out of the 20 categories proposed in [43], as well as other recent methods [38–40].

Other methods rely on datasets comprising images from a single diffusion-based generator, such as Latent Diffusion [7, 10, 11], Guided Diffusion [44] or Stable Diffusion [22, 37]. Prior work [7, 11] highlights the importance of aligning training and eval data in terms of semantic content. This choice allowed to better exploit the potential of fixed-pretraining CLIP features by strongly reducing the number of images needed for fine-tuning [11]. This strategy has the key merit of reducing the dataset content bias, thus allowing for better quality training, and is also adopted in other approaches both during training [1, 3] and test time to carry out a fairer evaluation [2].

Creating training data by artifact injection. A different line of research is to create simulated fake images by injecting traces of the generative process in real images. A seminal work along this line was done by Zhang et al. [52] for GAN image detection. The idea is to simulate artifacts shared by several generators. These peculiar traces are caused by the up-sampling processes included in the generation pipeline and show up as peaks in the frequency domain. Besides these frequency peaks, synthetic images, both GAN-based and diffusion-based, have been shown to exhibit spectral features that are very different from those of natural images [14, 15]. In fact, real images exhibit much richer spectral content at intermediate frequencies than synthetic ones [9, 46].

For GAN-generated images, producing realistic simulated fakes requires training the generation architecture specifically for this task [19, 52]. In contrast, diffusion-based image generation can leverage a pre-trained autoencoder embedded within the generation pipeline, which projects images into a latent space without the need for additional training [11, 29]. This procedure has been very recently used in a concurrent work [35] to reduce semantic biases during training (Fig. 3.c). Different from [35] we generate synthetic data by also performing the diffusion steps. Later in this work we will show that this choice allows us

Reference	# Real/ # Fake	Real Source	# Models
Synthbuster [2]	1k / 9k	RAISE	9
GenImage [53]	1.3M / 1.3M	ImageNet	8
FakeInversion [7]	44.7k / 44.7k	Internet	13
SynthWildX [11]	500 / 1.5k	X	3
WildRF [6]	1.25k / 1.25k	Reddit, FB, X	unknown

Table 1. Publicly available datasets we used for our evaluation.

to exploit even subtler inconsistencies at lower frequencies, enhancing the detector performance (Fig. 3.d).

3. Evaluation Protocol

3.1. Datasets

In our experimental analysis, we want to avoid or at least minimize the influence of any possible afore-mentioned biases. To this end, we carefully select the evaluation datasets as outlined below. Experiments on further datasets are provided in the supplementary material.

To avoid format bias, we use Synthbuster [2], where both real and generated images are saved in raw format. Therefore, a good performance on this dataset cannot come from the exploitation of JPEG artifacts. A complementary strategy to avoid format biases is to reduce the mismatch between real (compressed) and synthetic (uncompressed) images by compressing the latter. To this end, we modified the fake class in GenImage [53] by compressing images at a JPEG quality close to those used for the real class, as suggested in [18]. This modified dataset, referred to as GenImage unbiased, comprises 5k real and 5k fake images, a small fraction of the original dataset.

To avoid content bias, we also evaluate performance on datasets where fakes are generated using automated descriptions of real images. In studies like [2, 3] these descriptions are refined into manually created prompts for text-based generation. As a result, the generated images closely align with the content of the real images, minimizing possible biases due to semantic differences. A more refined dataset in this regard is FakeInversion [7], where real images are retrieved from the web using reverse image search, thus ensuring stylistic and thematic alignment with the fakes.

To allow in-the-wild analysis, we experiment also on datasets of real/fake images collected from the web, such as WildRF [6] and SynthWildX [11]. Both datasets comprise images coming from several popular social networks. Tags were used to find fake images on Reddit, Facebook and X. A short summary of all the datasets used in our evaluation is listed in Table 1.

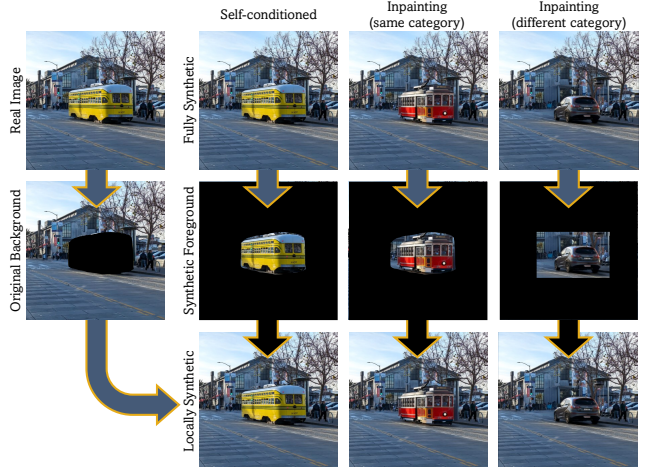


Figure 4. Content augmentation process. Starting with a real image, we use its generated variants (first row) and their locally manipulated versions (last row), created by replacing the original background. When inpainting with a different category, we use a bounding box instead of an object mask to allow space for new objects of varying shapes and sizes.

3.2. Metrics

Most work on GenAI image detection measure performance by means of threshold-independent metrics, such as Area Under the Curve (AUC) or average precision (AP). These metrics indicate ideal classification performance, however the optimal separating threshold is not known and, quite often, the balanced accuracy at a fixed threshold (e.g. 0.5) remains low, especially when there are significant differences between training and testing distributions [41]. Some papers address this problem by adjusting the threshold through a calibration procedure, assuming access to a few images from the synthetic generator under evaluation [10, 31, 43]. In a realistic situation, availability of such calibration images is uncertain.

In this work, to provide a comprehensive assessment of performance, we use both AUC and Accuracy at 0.5, in addition we compute the Expected Calibration Error (ECE) and the Negative Log-Likelihood (NLL). ECE measures the ability of a model to provide prediction probabilities well aligned with the true probabilities. More precisely, we use the Binary ECE, which is the weighted average of the differences between the actual probability and the predicted probability across different bins [32]. Then, we use the balanced NLL [33], which evaluates the similarity between the distribution of the model’s predictions and the actual data distribution, penalizing both low confidence in the correct class and overconfidence in incorrect ones. More details on these metrics can be found in the supplementary material.

Training settings		Synthbuster					New Generators		WildRF			AVG	
Training Set	Augmentation	Midjourney	SDXL	DALL-E 2	DALL-E 3	Firefly	FLUX	SD 3.5	Facebook	Reddit	Twitter	AUC \uparrow /bAcc \uparrow	
AUC / bAcc (%)	(b) paired by text	—	97.5 / 55.9	99.1 / 65.2	74.5 / 50.1	99.4 / 62.7	71.3 / 50.1	98.3 / 55.4	92.6 / 53.0	64.7 / 63.7	56.5 / 57.7	83.8 / 71.2	83.8 / 58.5
	(c) reconstructed	—	100. / 99.4	100. / 99.1	77.7 / 52.7	97.0 / 72.3	99.3 / 89.3	94.5 / 67.0	98.4 / 84.3	98.1 / 94.7	75.5 / 75.3	93.3 / 88.4	93.4 / 82.3
	(d) self-conditioned	—	99.8 / 96.9	99.7 / 96.6	89.4 / 58.1	97.9 / 82.5	100. / 99.1	89.5 / 57.6	98.9 / 89.6	95.6 / 90.6	79.3 / 75.5	94.2 / 89.0	94.4 / 83.6
	(d) self-conditioned	cutmix/mixup	99.5 / 96.1	99.4 / 95.4	81.2 / 58.9	96.7 / 82.5	99.9 / 98.2	81.9 / 56.8	97.7 / 88.3	95.5 / 90.3	80.4 / 76.8	93.3 / 87.7	92.5 / 83.1
	"	inpainted	100. / 96.8	100. / 96.8	81.2 / 65.0	99.1 / 95.1	100. / 96.8	94.3 / 84.9	99.6 / 95.9	99.0 / 87.5	81.0 / 70.5	96.7 / 86.1	95.1 / 87.5
	"	inpainted++	99.8 / 96.4	99.7 / 96.4	92.9 / 83.9	99.0 / 95.2	99.9 / 96.9	94.8 / 87.7	93.4 / 86.8	95.7 / 90.3	82.3 / 75.5	96.0 / 90.3	95.4 / 89.9
"	inpainted++	99.9 / 96.8	99.8 / 96.6	83.1 / 71.0	97.4 / 92.2	99.5 / 96.7	92.9 / 85.0	94.7 / 89.5	97.7 / 92.5	83.2 / 78.8	95.8 / 89.5	94.4 / 88.9	
NLL / ECE	Training Set	Augmentation	Midjourney	SDXL	DALL-E 2	DALL-E 3	Firefly	FLUX	SD 3.5	facebook	reddit	twitter	NLL \downarrow /ECE \downarrow
	(b) paired by text	—	2.21 / .427	1.41 / .342	4.83 / .496	1.45 / .364	5.04 / .498	2.10 / .429	3.06 / .460	1.83 / .300	2.66 / .366	1.41 / .253	2.60 / .393
	(c) reconstructed	—	0.02 / .006	0.02 / .006	4.27 / .463	1.13 / .263	0.29 / .104	1.66 / .316	0.60 / .150	0.23 / .046	1.82 / .221	0.62 / .096	1.07 / .167
	(d) self-conditioned	—	0.10 / .026	0.11 / .025	2.57 / .401	0.67 / .165	0.02 / .005	2.57 / .404	0.36 / .094	0.39 / .076	1.36 / .195	0.52 / .099	0.87 / .149
	(d) self-conditioned	cutmix/mixup	0.09 / .014	0.11 / .022	1.93 / .381	0.45 / .147	0.05 / .012	1.90 / .398	0.31 / .092	0.32 / .071	0.94 / .172	0.40 / .078	0.65 / .139
	"	inpainted	0.08 / .046	0.09 / .045	0.99 / .275	0.13 / .022	0.08 / .046	0.37 / .094	0.11 / .032	0.33 / .157	0.72 / .206	0.32 / .127	0.32 / .105
"	inpainted+	0.09 / .039	0.10 / .036	0.44 / .099	0.13 / .023	0.08 / .042	0.34 / .065	0.40 / .077	0.28 / .067	0.70 / .155	0.27 / .054	0.28 / .066	
"	inpainted++	0.11 / .060	0.11 / .061	0.68 / .193	0.22 / .040	0.13 / .064	0.36 / .076	0.29 / .040	0.20 / .031	0.54 / .111	0.26 / .071	0.29 / .075	

Table 2. Ablation study. We compare several forms of content alignment and content augmentation. Performance are in terms of AUC/Accuracy (top) and ECE/NLL (bottom). Note that all variants share a standard augmentation (blurring + JPEG compression) as proposed in [43]. For content alignment we consider the image pairing strategies described in Fig. 3: b) text-driven generation, c) reconstruction through autoencoder, and our proposal d) using self-conditioned images (through autoencoder and diffusion). For the last solution we test several forms of augmentation: a standard cutmix/mixup, and three proposed strategies based on inpainting: inpainted (same category and corresponding local version), inpainted+ (both same and different categories and corresponding local versions), and inpainted++ (like inpainted+ with further augmentation operations, such as scaling, cut-out, noise addition, and jittering).

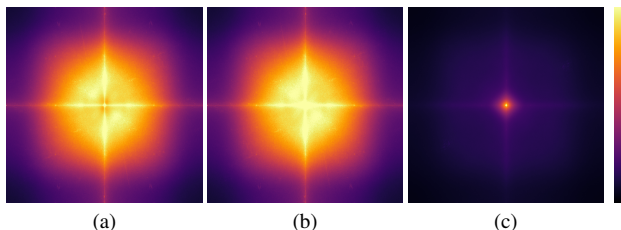


Figure 5. Power spectra computed by averaging (2000 images) the differences between: (a) real and reconstructed images, (b) real and self-conditioned images, and (c) reconstructed and self-conditioned images. We can observe that the self-conditioned generation embeds forensic artifacts even at lower frequencies compared to reconstructed images. This means that it is possible to better exploit such inconsistencies to distinguish real from fakes.

4. Proposed Method

To realize and test our bias-free training paradigm we:

- build a dataset consisting of real and generated fake images, where the latter are well aligned with their real counterparts but include the forensic artifacts of the diffusion-based generation process. The dataset is then enriched through several forms of augmentation, including locally inpainted images, and comprises eventually 309,102 generated images.
- use this aligned dataset to fine-tune a Vision Transformer (ViT)-based model end-to-end. The model processes the entire (512×512) input image, so we avoid resizing and cropping operations altogether during fine-tuning. At inference time, 512×512 crops are extracted from the image (if the image is larger we average the results of multiple crops).

Specifically, we use the image embedding network from the SigLIP model proposed in [49]. This model is pre-trained for image-text matching but employs a pairwise sigmoid loss instead of the softmax loss function used in CLIP models. This modification improves memory efficiency, enabling the use of larger batch sizes and input dimensions. The dataset instead is created starting from the images collected from the training set of MS-COCO dataset [26], for a total of 51,517 real images.

To ensure fake images semantically match the content of real images, we exploit the conditioning mechanism of Stable Diffusion models that allows us to control the synthesis process through a side input, which can be a class-label, a text or another image. The side input is firstly projected to an intermediate representation by a domain specific encoder, and then feeds the intermediate layers of the autoencoders for denoising in the embedding space. After several denoising steps, a decoder is used to obtain the conditioned synthetic image from embedded vector (See Fig. 1). In our self-conditioned generation, we use the inpainting diffusion model of Stable Diffusion 2.1 [36], that has three side inputs: the reference image, a binary mask of the area to inpaint, and a textual description. Using an empty mask, we induce the diffusion steps to regenerate the input, that is, to generate a new image with exactly the same content of the input image. For the content augmentation process, we use the Stable Diffusion 2.1 inpainting method to replace an object with a new one, chosen from the same category or from a different one. Moreover, as shown in Fig. 4, besides the default inpainting, which regenerates the whole image, we consider also a version where the original background is restored. Note that during training, we balance the real and fake class taking an equal number of images from each.

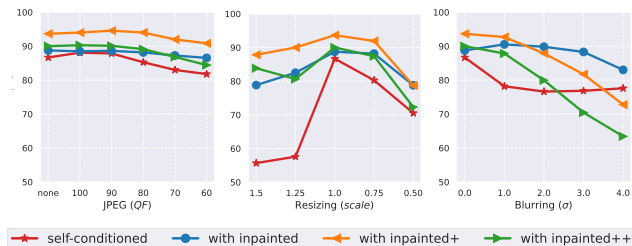


Figure 6. Robustness analysis in terms of balanced Accuracy carried out on nine generators of Synthbuster dataset [2].

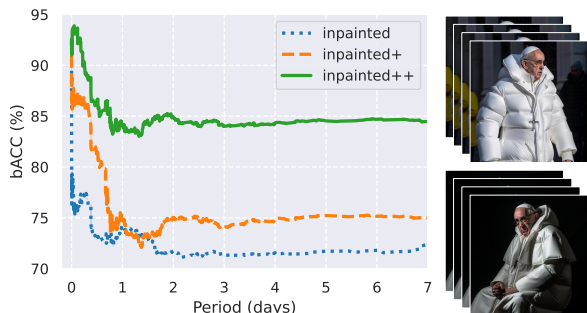


Figure 7. Balanced accuracy of B-Free under various augmentation strategies evaluated from the initial online post. We analyzed multiple web-scraped versions of real and fake images that went viral on internet.

In the following, we present our ablation study. To avoid dataset bias we use the WildRF [6] and Synthbuster [2] datasets, as explained in Section 3. In addition, we test on 1000 FLUX and 1000 Stable Diffusion 3.5 images, to verify performance on some of the latest synthetic generators.

4.1. Influence of content alignment

In Tab. 2 we show the performance achieved with different dataset alignment strategies, as described in Fig. 3. Note that all variants are trained with standard augmentations, including blurring and JPEG compression, as proposed in [43]. From the Table, we can observe that there is a large gain in terms of both AUC ($\simeq 10\%$) and balanced accuracy ($\simeq 20\%$) when upgrading from a text-driven generation (first row) to a solution where real and fake images share the semantic content, both reconstructed and self conditioned (see Fig. 3 for approaches). The proposed solution of using a diffusion pass demonstrates further improvement across all the evaluation metrics. This is highlighted in Fig. 5, where we show the power spectra evaluated by averaging the difference between the real and reconstructed images and the real and self-conditioned images. We observe that self-conditioned generation introduces forensic artifacts even at the lowest frequencies, indicating a detector trained on such images can exploit inconsistencies on a broader range of frequencies.

Training Set	Architecture	FT	AUC \uparrow	bAcc \uparrow	NLL \downarrow	ECE \downarrow
Ours	SigLip 512	e2e	95.4	89.9	0.28	.066
Ours	SigLip 512	LP	63.7	52.2	0.91	.285
Ours	CLIP/ViT-L 224	e2e	75.2	73.9	0.66	.225
LDM [10]	CLIP/ViT-L 224	e2e	63.9	48.5	3.39	.487
ProGAN [43]	CLIP/ViT-L 224	e2e	54.7	45.2	4.85	.525

Table 3. Ablation study on the influence of the network architecture and the training data. We compare our solution, SigLip model trained end-to-end with content augmentation, with: fine-tuning (FT) of the last linear layer (linear probing, LP) a CLIP-based network and two well-known public training datasets: one based on ProGAN [43] and the other on Latent Diffusion [10].

4.2. Effect of content augmentation

We also analyze the effect of different content augmentation strategies (Fig. 4). We consider standard operations like cut-mix [48] and mix-up [51] and compare them with our proposed solutions that include three variants:

- *inpainted*, we replace an object with another from the same category plus the version where the background is substituted with pristine pixels (effectively a local image edit);
- *inpainted+*, we replace an object with another from both the same and a different category plus the corresponding versions where the background is substituted with pristine pixels;
- *inpainted++*, we further add some more standard augmentation operations, such as scaling, cut-out, noise addition, and jittering.

Overall, it is evident from Tab. 2 that augmentation plays a critical role in enhancing model generalization and this can be appreciated especially by looking at balanced accuracy and calibration measures. In fact, all of them improve significantly, while AUC is almost constant. More specifically, accuracy increases on average from around 83% to 89% thanks to our content-based augmentation. The most significant gains are observed on DALL-E 2, DALL-E 3 and FLUX that, probably, differ the most from Stable 2.1 in terms of architecture and hence require a stronger augmentation strategy to generalize.

Robustness. In Fig. 6, we analyze the impact of our content augmentation, assessing robustness under various operations: JPEG compression, resizing, and blurring. Compared to using only self-conditioned images, all three proposed variants of augmentation offer a clear advantage, especially when resizing is applied. However, we can notice that in this experiment, the strongest augmentation strategy (*inpainted++*) may appear useless. Indeed, the relevance of such aggressive augmentation is more evident when analyzing images over the web. In fact, distinguishing real from synthetic images on social networks may be especially challenging due to the presence of multiple re-posting that impair image quality over time. A recent study conducted in

bAcc(%) \uparrow /NLL \downarrow	Synthbuster					New Generators		WildRF			AVG
	Midjourney	SDXL	DALL-E 2	DALL-E 3	Firefly	FLUX	SD 3.5	Facebook	Reddit	Twitter	bAcc \uparrow /NLL \downarrow
CNNDetect	49.5 / 8.45	49.8 / 6.90	50.2 / 5.75	49.5 / 12.9	50.3 / 3.66	49.5 / 10.1	50.0 / 5.30	50.0 / 9.84	50.7 / 6.66	50.1 / 8.64	50.0 / 7.83
DMID	100. / 0.00	99.7 / 0.01	50.1 / 5.99	50.0 / 7.08	51.0 / 1.72	63.7 / 1.27	99.9 / 0.01	87.8 / 0.52	74.3 / 1.82	79.1 / 0.85	75.6 / 1.93
LGrad	57.7 / 6.88	58.5 / 6.81	55.6 / 7.10	47.9 / 7.58	47.4 / 7.50	54.9 / 7.11	51.9 / 7.24	66.6 / 3.74	57.8 / 4.72	45.7 / 5.31	54.4 / 6.40
UnivFD	52.4 / 2.35	68.0 / 1.15	83.5 / 0.43	47.3 / 3.94	90.7 / 0.24	48.4 / 3.45	69.3 / 1.07	48.8 / 3.06	59.5 / 1.37	56.0 / 2.01	62.4 / 1.91
DeFake	69.7 / 0.72	76.3 / 0.56	64.0 / 0.92	84.9 / 0.36	72.4 / 0.63	79.2 / 0.46	81.2 / 0.42	66.3 / 0.89	65.9 / 0.82	63.4 / 0.94	72.3 / 0.67
DIRE	49.7 / 15.3	49.9 / 15.3	50.0 / 15.3	50.0 / 15.3	49.9 / 15.3	50.0 / 15.3	50.0 / 15.3	51.9 / 4.98	79.5 / 2.15	56.7 / 4.39	53.7 / 11.9
AntifakePrompt	70.4 / -	84.7 / -	65.5 / -	86.0 / -	70.0 / -	59.6 / -	60.7 / -	69.7 / -	68.9 / -	78.0 / -	71.3 / -
NPR	44.9 / 16.6	50.3 / 16.2	50.2 / 16.2	0.6 / 29.9	0.4 / 47.3	50.3 / 16.2	50.3 / 16.2	50.0 / 32.2	78.3 / 9.39	51.8 / 25.2	42.7 / 22.5
FatFormer	44.4 / 5.22	66.7 / 2.76	54.1 / 3.64	35.9 / 6.90	60.1 / 3.59	39.4 / 6.10	49.1 / 5.06	54.7 / 4.54	69.5 / 2.54	54.8 / 4.40	52.9 / 4.48
FasterThanLies	61.3 / 2.98	71.1 / 1.79	50.8 / 5.15	53.5 / 3.79	55.2 / 4.40	53.8 / 4.10	53.7 / 3.76	46.2 / 3.32	51.0 / 3.99	53.9 / 3.31	55.1 / 3.66
RINE	54.6 / 5.03	71.8 / 1.99	82.2 / 0.77	45.3 / 20.5	91.2 / 0.36	46.7 / 10.1	81.3 / 1.22	52.8 / 6.51	67.7 / 2.46	56.0 / 5.23	65.0 / 5.43
AIDE	57.5 / 0.95	68.4 / 0.70	34.9 / 1.34	33.7 / 1.38	24.8 / 2.00	62.9 / 0.82	63.3 / 0.82	56.9 / 0.94	72.1 / 0.62	57.3 / 1.01	53.2 / 1.06
LaDeDa	50.7 / 24.8	50.7 / 24.8	50.5 / 24.8	41.1 / 25.4	47.4 / 25.6	50.5 / 24.8	50.7 / 24.8	70.3 / 7.19	74.7 / 7.93	59.6 / 9.40	54.6 / 19.9
C2P-CLIP	52.8 / 1.10	77.7 / 0.48	55.6 / 0.99	63.2 / 0.73	59.5 / 0.89	50.1 / 1.30	60.9 / 0.93	54.4 / 0.97	68.4 / 0.67	57.4 / 0.91	60.0 / 0.90
CoDE	76.9 / 0.82	75.2 / 0.81	54.6 / 2.44	73.2 / 0.98	58.6 / 2.00	59.8 / 1.97	67.7 / 1.27	70.0 / 0.97	66.1 / 1.29	70.9 / 1.01	67.3 / 1.36
Ours	96.4 / 0.09	96.4 / 0.10	83.9 / 0.44	95.2 / 0.13	96.9 / 0.08	87.7 / 0.34	86.8 / 0.40	90.3 / 0.28	75.5 / 0.70	90.3 / 0.27	89.9 / 0.28

Table 4. Comparison with SoTA methods in terms of balanced Accuracy and balanced NLL across different generators. Note that AntifakePrompt [8] provides only hard binary labels hence calibration measures cannot be computed.

[20] analyzed the detector behavior on different instances of an image shared online, showing that the performance degrades noticeably in time due to repeated re-posting. To better understand the impact of our augmentation strategies on such images, we collected a total of 900 real/fake images that went viral, including several versions of the same real or fake image. In Fig. 7 we show the balanced accuracy for our augmentation strategies, evaluated in different time periods from the first online post. In all cases the balanced accuracy gets significantly worse after just one day, but our strategy with more aggressive augmentation succeeds in stabilizing the performance to a very good level, always above 85%. This analysis makes clear that when testing the detector on images from the web a more intense augmentation *inpainted++* is needed, otherwise the variant *inpainted+* is sufficient. For remaining experiments, *Ours* refers to the detector trained using *inpainted+* augmentation.

4.3. Influence of training data

We conduct additional experiments to gain deeper insights into the impact of the chosen architecture and the proposed training data on the same datasets shown in Tab. 2. First, we compare our adopted model, SigLIP trained end-to-end, with an alternative fine-tuning strategy that involves training only the final linear layer, known as linear probing (LP) that is largely adopted in the literature [11, 31]. From Tab. 3 we can see that this latter solution does not perform well. One possible explanation is that features from last layer capture high-level semantics, while our dataset is built to exploit low-level artifacts that derive from first and intermediate layers [10, 21]. Then we use a different architecture, a CLIP-based model that works with an input size equal to 224×224 , and vary the training dataset by including two well known datasets largely used in the literature, one

Ref.	Acronym	Training Real/Fake	Size (K)	Aug.
[43]	CNNDetect	LSUN / ProGAN	360 / 360	✓
[10]	DMID	COCO, LSUN / Latent	180 / 180	✓
[38]	LGrad	LSUN / ProGAN	72 / 72	✓
[31]	UnivFD	LSUN / ProGAN	360 / 360	✓
[37]	DeFake	COCO / SD	20 / 20	
[44]	DIRE	LSUN-Bed / ADM	40 / 40	
[8]	AntifakePrompt	COCO / SD3,SD2-inp	90 / 60	✓
[39]	NPR	LSUN / ProGAN	72 / 72	
[27]	FatFormer	LSUN / ProGAN	72 / 72	
[22]	FasterThanLies	COCO / SD	108 / 542	✓
[21]	RINE	LSUN / ProGAN	72 / 72	✓
[45]	AIDE	ImageNet / SD 1.4	160 / 160	✓
[6]	LaDeDa	LSUN / ProGAN	360 / 360	
[40]	C2P-CLIP	LSUN / ProGAN	72 / 72	✓
[3]	CoDE	LAION / SD1.4, SD2.1, SDXL, DeepF. IF	2.3M / 9.2M	✓

Table 5. AI-generated image detection methods used for comparison and whose code is made publicly available. We specify the source and size of the training dataset, and whether augmentation is applied.

based on ProGAN [43] and the other on Latent Diffusion [10]. First we note that our training paradigm achieves the best performance over all the metrics, with a very large gain (+17% in bAcc). This is due to the adoption of a model that can handle a larger input size up to 512×512 and hence can process at once the entire image of our training set.

5. Comparison with the State-of-The-Art

In this Section, we conduct a comparison with SoTA methods on 27 diverse synthetic generation models. To ensure fairness, we include only SoTA methods with publicly available code and/or pre-trained models. The selected methods are listed in Table 5 and are further described in the supplementary material together with additional experiments.

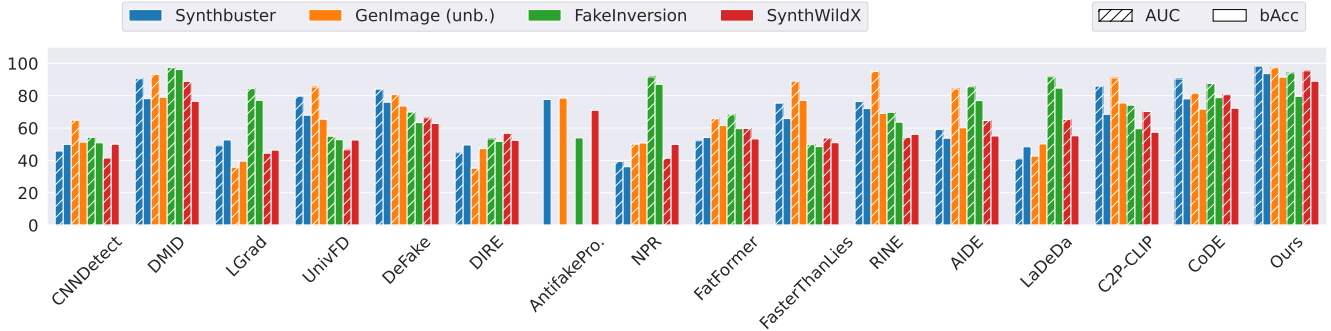


Figure 8. Average performance in term of AUC and balanced accuracy of SoTA methods on four datasets: Synthbuster, GenImage, FakeInversion, SynthWildX.

A first experiment is summarized in Tab. 4 with results given in terms of balanced accuracy and NLL. Most of the methods struggle to achieve a good accuracy, especially on more recent generators. Instead, B-Free obtains a uniformly good performance on all generators, irrespective of the image origin, whether they are saved in raw format or downloaded from social networks, outperforming the second best (see last column) by +14.3% in bACC and +58% in NLL. Then, we evaluate again all methods on GenImage (unbiased), FakeInversion [7], and SynthWildX [11]. As these datasets encompass multiple generators, we only report the average performance in Tab. 6. On these additional datasets, most methods provide unsatisfactory results, especially in the most challenging scenario represented by SynthWildX, with images that are shared over the web. The proposed method performs well on all datasets, just a bit worse on FakeInversion. Finally in Fig. 8 we study how AUC compares with balanced accuracy for all the methods over several datasets. We observe that some methods, like NPR and LGrad, present a clear non-uniform behavior, with very good performance on a single dataset and much worse on the others. This seems to suggest that these methods may not be truly detecting forensic artifacts, instead are rather exploiting intrinsic biases within the dataset. Differently, the proposed method presents a uniform performance across all datasets and a very small loss between AUC and accuracy.

6. Limitations

The method proposed in this work is trained using fake images that are self-conditioned reconstructions from Stable Diffusion 2.1 model. If new generators will be deployed in the future that have a completely different synthesis process, then is it very likely that this approach will fail (the principles and ideas shared in this work may still hold). Further, being a data-driven approach it can be adversarially attacked by a malicious user. This is a very relevant issue that we plan to address in our future work.

bAcc(%) \uparrow /NLL \downarrow	GenImage	FakeInver.	SynthWildX	AVG
CNNDetect	51.3 / 7.88	50.9 / 7.94	50.0 / 8.08	50.7 / 7.96
DMID	79.0 / 1.66	96.1 / 0.25	76.6 / 0.82	83.9 / 0.91
LGrad	39.6 / 7.12	77.2 / 2.27	46.3 / 5.53	54.3 / 4.97
UnivFD	65.5 / 1.31	52.8 / 2.19	52.5 / 2.55	56.9 / 2.02
DeFake	73.7 / 0.74	63.3 / 0.95	62.9 / 0.98	66.6 / 0.89
DIRE	47.3 / 6.54	51.8 / 13.4	52.5 / 4.60	50.5 / 8.19
AntifakePrompt	78.5 / -	53.9 / -	70.8 / -	67.8 / -
NPR	50.7 / 25.3	87.0 / 4.96	49.9 / 28.2	62.6 / 19.5
FatFormer	61.5 / 3.99	59.7 / 3.45	53.3 / 4.75	58.2 / 4.06
FasterThanLies	77.0 / 1.23	48.6 / 3.64	50.9 / 3.40	58.8 / 2.76
RINE	69.1 / 2.57	63.6 / 4.84	56.2 / 6.07	63.0 / 4.49
AIDE	60.2 / 1.01	76.9 / 0.54	55.0 / 1.05	64.0 / 0.86
LaDeDa	50.2 / 29.2	84.7 / 3.03	55.1 / 10.2	63.3 / 14.1
C2P-CLIP	75.5 / 0.57	59.6 / 0.82	57.4 / 0.91	64.2 / 0.76
CoDE	71.7 / 1.43	78.8 / 0.74	72.3 / 0.95	74.2 / 1.04
Ours	91.4 / 0.27	79.6 / 0.76	89.0 / 0.30	86.7 / 0.44

Table 6. Comparison with SoTA methods in terms of average performance in terms of balanced accuracy and NLL for three additional datasets: GenImage, FakeInversion and SynthWildX.

7. Conclusions

In this work, we propose a new training paradigm for AI-generated image detection. First of all, we empirically demonstrate the importance of pairing real and fake images by constraining them to have the same semantic content. This helps to better extract common artifacts shared across diverse synthetic generators. Then we find that using aggressive data augmentation, in the form of partial manipulations, further boosts performance both in term of accuracy and of calibration metrics. This is extremely relevant especially when working in realistic scenarios, such as image sharing over social networks. Our findings emphasize that careful dataset curation and proper training strategy can be more impactful compared to developing more complex algorithms. We hope this work will inspire other researchers in the forensic community to pursue a similar direction, fostering advancements in bias-free training strategies.

Acknowledgments. We gratefully acknowledge the support of this research by a Google Gift. In addition, this work has received funding from the European Union under the Horizon Europe vera.ai project, Grant Agreement number 101070093, and was partially supported by SERICS (PE00000014) under the MUR National Recovery and Resilience Plan, funded by the European Union - NextGenerationEU.

References

- [1] Roberto Amoroso, Davide Morelli, Marcella Cornia, Lorenzo Baraldi, Alberto Del Bimbo, and Rita Cucchiara. Parents and Children: Distinguishing Multimodal DeepFakes from Natural Images. *ACM Trans. Multimedia Comput. Commun. Appl.*, 2024. 3
- [2] Quentin Bammey. Synthbuster: Towards detection of diffusion model generated images. *IEEE Open Journal of Signal Processing*, 2023. 2, 3, 4, 6, 14
- [3] Lorenzo Baraldi, Federico Cocchi, Marcella Cornia, Lorenzo Baraldi, Alessandro Nicolosi, and Rita Cucchiara. Contrasting Deepfakes Diffusion via Contrastive Learning and Global-Local Similarities. In *ECCV*, 2024. 2, 3, 4, 7, 12, 13
- [4] Clark Barrett, Brad Boyd, Elie Burzstein, Nicholas Carlini, Brad Chen, Jihye Choi, Amrita Roy Chowdhury, Mihai Christodorescu, Anupam Datta, Soheil Feizi, et al. *Identifying and Mitigating the Security Risks of Generative AI*. Now Foundations and Trends, 2024. 1
- [5] Giuseppe Cattaneo and Gianluca Roscigno. A possible pitfall in the experimental analysis of tampering detection algorithms. In *NBiS*, 2014. 2
- [6] Bar Cavia, Eliahu Horwitz, Tal Reiss, and Yedid Hoshen. Real-Time Deepfake Detection in the Real-World. *arXiv preprint arXiv:2406.09398*, 2024. 4, 6, 7, 12
- [7] George Cazenavette, Avneesh Sud, Thomas Leung, and Ben Usman. FakeInversion: Learning to Detect Images from Unseen Text-to-Image Models by Inverting Stable Diffusion. In *CVPR*, pages 10759–10769, 2024. 2, 3, 4, 8, 14, 15
- [8] You-Ming Chang, Chen Yeh, Wei-Chen Chiu, and Ning Yu. AntifakePrompt: Prompt-Tuned Vision-Language Models are Fake Image Detectors. *arXiv preprint arXiv:2310.17419*, 2023. 7, 12
- [9] Riccardo Corvi, Davide Cozzolino, Giovanni Poggi, Koki Nagano, and Luisa Verdoliva. Intriguing properties of synthetic images: from generative adversarial networks to diffusion models. In *CVPR Workshops*, pages 973–982, 2023. 3
- [10] Riccardo Corvi, Davide Cozzolino, Giada Zingarini, Giovanni Poggi, Koki Nagano, and Luisa Verdoliva. On the detection of synthetic images generated by diffusion models. In *ICASSP*, pages 1–5, 2023. 3, 4, 6, 7, 11, 12, 13
- [11] Davide Cozzolino, Giovanni Poggi, Riccardo Corvi, Matthias Nießner, and Luisa Verdoliva. Raising the Bar of AI-generated Image Detection with CLIP. In *CVPR Workshops*, pages 4356–4366, 2024. 2, 3, 4, 7, 8
- [12] Duc-Tien Dang-Nguyen, Cecilia Pasquini, Valentina Conotter, and Giulia Boato. RAISE: a raw images dataset for digital image forensics. In *ACM Multimedia Systems Conference*, page 219–224. Association for Computing Machinery, 2015. 2
- [13] Jing Dong, Wei Wang, and Tieniu Tan. CASIA image tampering detection evaluation database. In *IEEE ChinaSIP*, 2013. 2
- [14] Ricard Durall, Margret Keuper, and Janis Keuper. Watch your up-convolution: CNN based Generative Deep Neural Networks are failing to reproduce spectral distributions. In *CVPR*, pages 7890–7899, 2020. 3
- [15] Tarik Dzanic, Karan Shah, and Freddie Witherden. Fourier spectrum discrepancies in deep network generated images. In *NeurIPS*, pages 3022–3032, 2020. 3
- [16] Ziv Epstein, Aaron Hertzmann, et al. Art and the science of generative AI. *Science*, 380(6650):1110–1111, 2023. 1
- [17] Diego Gragnaniello, Davide Cozzolino, Francesco Marra, Giovanni Poggi, and Luisa Verdoliva. Are GAN generated images easy to detect? A critical analysis of the state-of-the-art. In *ICME*, pages 1–6, 2021. 2
- [18] Patrick Grommelt, Louis Weiss, Franz-Josef Pfreundt, and Janis Keuper. Fake or JPEG? Revealing Common Biases in Generated Image Detection Datasets. *arXiv preprint arXiv:2403.17608*, 2024. 2, 4
- [19] Yonghyun Jeong, Doyeon Kim, Youngmin Ro, Pyounggeon Kim, and Jongwon Choi. FingerprintNet: Synthesized Fingerprints for Generated Image Detection. In *ECCV*, pages 76–94, 2022. 3
- [20] Dimitrios Karageorgiou, Quentin Bammey, Valentin Porcellini, Bertrand Goupil, Denis Teyssou, and Symeon Papadopoulos. Evolution of Detection Performance throughout the Online Lifespan of Synthetic Images. In *ECCV Workshops*, 2024. 7
- [21] Christos Koutlis and Symeon Papadopoulos. Leveraging Representations from Intermediate Encoder-blocks for Synthetic Image Detection. In *ECCV*, 2024. 2, 3, 7, 12, 13
- [22] Romeo Lanzino, Federico Fontana, Anxhelo Diko, Marco Raoul Marini, and Luigi Cinque. Faster Than Lies: Real-time Deepfake Detection using Binary Neural Networks. In *CVPR Workshops*, pages 3771–3780, 2024. 3, 7, 12
- [23] Yanhao Li, Quentin Bammey, Marina Gardella, Tina Nikoukhah, Jean-Michel Morel, Miguel Colom, and Rafael Grompone Von Gioi. MaskSim: Detection of Synthetic Images by Masked Spectrum Similarity Analysis. In *CVPR*, pages 3855–3865, 2024. 14
- [24] Yixuan Li, Xuelin Liu, Xiaoyang Wang, Shiqi Wang, and Weisi Lin. FakeBench: Uncover the Achilles’ Heels of Fake Images with Large Multimodal Models. *arXiv preprint arXiv:2404.13306*, 2024. 14
- [25] Li Lin, Neeraj Gupta, Yue Zhang, Hainan Ren, Chun-Hao Liu, Feng Ding, Xin Wang, Xin Li, Luisa Verdoliva, and Shu Hu. Detecting multimedia generated by large AI models: A survey. *arXiv preprint arXiv:2204.06125*, 2024. 1
- [26] Tsung-Yi Lin, Michael Maire, Serge Belongie, James Hays, Pietro Perona, Deva Ramanan, Piotr Dollár, and C. Lawrence

- Zitnick. Microsoft COCO: Common objects in context. In *ECCV*, pages 740–755, 2014. 5
- [27] Huan Liu, Zichang Tan, Chuangchuang Tan, Yunchao Wei, Jingdong Wang, and Yao Zhao. Forgery-aware Adaptive Transformer for Generalizable Synthetic Image Detection. In *CVPR*, pages 10770–10780, 2024. 2, 3, 7, 12
- [28] Zhuang Liu and Kaiming He. A Decade’s Battle on Dataset Bias: Are We There Yet? *arXiv preprint arXiv:2403.08632v1*, 2024. 2
- [29] Sara Mandelli, Paolo Bestagini, and Stefano Tubaro. When Synthetic Traces Hide Real Content: Analysis of Stable Diffusion Image Laundering. *arXiv preprint arXiv:2407.10736*, 2024. 3
- [30] Francesco Marra, Diego Gragnaniello, Luisa Verdoliva, and Giovanni Poggi. Do GANs Leave Artificial Fingerprints? In *MIPR*, pages 506–511, 2019. 2
- [31] Utkarsh Ojha, Yuheng Li, and Yong Jae Lee. Towards universal fake image detectors that generalize across generative models. In *CVPR*, pages 24480–24489, 2023. 1, 2, 3, 4, 7, 12
- [32] Mahdi Pakdaman Naeni, Gregory Cooper, and Milos Hauskrecht. Obtaining Well Calibrated Probabilities Using Bayesian Binning. *AAAI*, 29(1), 2015. 4
- [33] Joaquin Quiñero-Candela, Ido Dagan, Bernardo Magnini, and Florence D’Alché-Buc. *Machine Learning Challenges: Evaluating Predictive Uncertainty, Visual Object Classification, and Recognizing Textual Entailment*. Springer, 2006. 4
- [34] Alec Radford, JongWook Kim, Chris Hallacy, Aditya Ramesh, Gabriel Goh, Sandhini Agarwal, Girish Sastry, Amanda Askell, Pamela Mishkin, Jack Clark, et al. Learning Transferable Visual Models From Natural Language Supervision. In *ICML*, pages 8748–8763, 2021. 1
- [35] Anirudh Sundara Rajan, Utkarsh Ojha, Jedidiah Schloesser, and Yong Jae Lee. On the Effectiveness of Dataset Alignment for Fake Image Detection. *arXiv preprint arXiv:2410.11835*, 2024. 2, 3
- [36] Robin Rombach, Andreas Blattmann, Dominik Lorenz, Patrick Esser, and Björn Ommer. Stable Diffusion. <https://github.com/Stability-AI/stablediffusion>, 2022. 5
- [37] Zeyang Sha, Zheng Li, Ning Yu, and Yang Zhang. DE-FAKE: Detection and Attribution of Fake Images Generated by Text-to-Image Generation Models. In *ACM SIGSAC*, pages 3418–3432, 2023. 3, 7, 12
- [38] Chuangchuang Tan, Yao Zhao, Shikui Wei, Guanghua Gu, and Yunchao Wei. Learning on Gradients: Generalized Artifacts Representation for GAN-Generated Images Detection. In *CVPR*, pages 12105–12114, 2023. 3, 7, 11
- [39] Chuangchuang Tan, Huan Liu, Yao Zhao, Shikui Wei, Guanghua Gu, Ping Liu, and Yunchao Wei. Rethinking the Up-Sampling Operations in CNN-based Generative Network for Generalizable Deepfake Detection. In *CVPR*, 2024. 7, 12
- [40] Chuangchuang Tan, Renshuai Tao, Huan Liu, Guanghua Gu, Baoyuan Wu, Yao Zhao, and Yunchao Wei. C2P-CLIP: Injecting Category Common Prompt in CLIP to Enhance Generalization in Deepfake Detection. *arXiv preprint arXiv:2408.09647*, 2024. 3, 7, 12
- [41] Diangarti Tariang, Riccardo Corvi, Davide Cozzolino, Giovanni Poggi, Koki Nagano, and Luisa Verdoliva. Synthetic Image Verification in the Era of Generative AI: What Works and What Isn’t There Yet. *IEEE Security & Privacy*, 22: 37–49, 2024. 1, 4
- [42] Antonio Torralba and Alexei A. Efros. Unbiased look at dataset bias. In *CVPR*, 2011. 2
- [43] Sheng-Yu Wang, Oliver Wang, Richard Zhang, Andrew Owens, and Alexei A Efros. CNN-generated images are surprisingly easy to spot... for now. In *CVPR*, pages 8695–8704, 2020. 3, 4, 5, 6, 7, 11, 12, 13
- [44] Zhendong Wang, Jianmin Bao, Wengang Zhou, Weilun Wang, Hezhen Hu, Hong Chen, and Houqiang Li. DIRE for diffusion-generated image detection. In *ICCV*, pages 22445–22455, 2023. 3, 7, 12
- [45] Shilin Yan, Ouxiang Li, Jiayin Cai, Yanbin Hao, Xiaolong Jiang, Yao Hu, and Weidi Xie. A Sanity Check for AI-generated Image Detection. *arXiv preprint arXiv:2406.19435*, 2024. 7, 12
- [46] Xingyi Yang, Daquan Zhou, Jiashi Feng, and Xinchao Wang. Diffusion Probabilistic Model Made Slim. In *CVPR*, pages 22552–22562, 2023. 3
- [47] Ning Yu, Larry S Davis, and Mario Fritz. Attributing Fake Images to GANs: Learning and Analyzing GAN Fingerprints. In *ICCV*, pages 7556–7566, 2019. 2
- [48] Sangdoon Yun, Dongyoon Han, Seong Joon Oh, Sanghyuk Chun, Junsuk Choe, and Youngjoon Yoo. CutMix: Regularization strategy to train strong classifiers with localizable features, 2019. 6
- [49] Xiaohua Zhai, Basil Mustafa, Alexander Kolesnikov, and Lucas Beyer. Sigmoid loss for language image pre-training. In *ICCV*, pages 11975–11986, 2023. 5, 12, 13
- [50] Fangneng Zhan, Yingchen Yu, Rongliang Wu, Jiahui Zhang, Shijian Lu, Lingjie Liu, Adam Kortylewski, Christian Theobalt, and Eric Xing. Multimodal Image Synthesis and Editing: The Generative AI Era. *IEEE TPAMI*, 45(12): 15098–15119, 2021. 1
- [51] Hongyi Zhang, Moustapha Cisse, Yann N. Dauphin, and David Lopez-Paz. mixup: Beyond Empirical Risk Minimization, 2018. 6
- [52] Xu Zhang, Svebor Karaman, and Shih-Fu Chang. Detecting and Simulating Artifacts in GAN Fake Images. In *WIFS*, 2019. 3
- [53] Mingjian Zhu, Hanting Chen, Qiangyu Yan, Xudong Huang, Guanyu Lin, Wei Li, Zhijun Tu, Hailin Hu, Jie Hu, and Yunhe Wang. GenImage: A Million-Scale Benchmark for Detecting AI-Generated Image. *NeurIPS*, 36:77771–77782, 2023. 4

A Bias-Free Training Paradigm for More General AI-generated Image Detection

Supplementary Material

In this supplementary document, we report more details about our implementation (Sec. 8). Moreover, we briefly describe the state of the art methods we compare to (Sec. 9), and give more details about the calibration metrics used in the experiments (Sec. 10). We also provide additional ablation results in Sec. 11 and carry out further experiments on generalization (Sec. 12) on additional publicly available datasets. Furthermore, we provide more results on the robustness of our approach compared with SoTA methods (Sec. 13).

8. Implementation Details

Training strategy. The proposed model leverages the SigLIP 512×512 image embedding network as its backbone, followed by two fully connected layers. The model is trained end-to-end using the binary cross-entropy loss function on an NVIDIA A100 GPU. The training process employs the ADAM optimizer with a learning rate of 1e-6, a weight decay of 1e-6, and a batch size of 24. During training, the balanced accuracy is evaluated on a validation set every 3435 iterations. Early stopping is applied to prevent overfitting: training is completed if the validation balanced accuracy does not improve by at least 0.1% over five consecutive evaluations.

Test strategy. If the test image is less than 512 pixels, padding is applied after patch embedding. Otherwise, we average the logit score over multiple crops to analyze the whole image.

Training Dataset. Here we give more details on how we built our dataset. Starting from the MS-COCO training set, consisting of 118K images with 80 categories of objects, we first discarded images with licenses different than Creative Commons. Before editing the images, we extracted the largest central crop, which allows us to retain most of the semantic content of the original image. We discarded images where objects are not present and ended up with a pristine source of 51,517 images. For content augmentation, we replaced the selected object with an object generated from the same category using the COCO segmentation mask, and from a different category using a rectangular box. We took care to not affect too much the realism of the content, so for the “different category” case the object is changed with one from a similar category, that belongs to the same COCO supercategory. In this scenario, the only exception is the category *person*, which does not have a supercategory and it is therefore replaced with a random object. As mentioned in the main paper, besides the default



Figure 9. Examples of content augmented images from our training dataset. From real images (first row), we generate inpainted versions with the same content (second row) and different content (third row).

inpainting, we also consider a version where we take the pixels of the object from the generated image, and the pixels of the background from the original one. We did the same with the self-conditioned image, restoring the background with original pixels. Therefore, we ended up with six fake versions for each real image (Fig. 4 of the main paper).

9. SoTA Methods

Below we provide a brief description of the methods we included in the comparison in Section 5 of our main paper. The training datasets used by these methods are indicated in Table 5 of the main paper.

CNNDetect [43]. This is a CNN-based detector built on ResNet50 (pre-trained on ImageNet) that adopts augmentation in the form of post-processing operations, such as blurring and compression.

DMID [10]. This work also relies on a ResNet-50, but it prevents down-sampling at the first layer so as to preserve the invisible forensics clues as much as possible, and uses a stronger augmentation to increase robustness.

LGrad [38]. This work is also based on a ResNet-50 classifier, but this is fed by a generalized artifacts representation of the image in the form of gradients. This representation is designed to more effectively capture the artifacts introduced by synthetic generators.

		Synthbuster					New Generators		WildRF			AVG	
Method	Training settings	Midjourney	SDXL	DALL-E 2	DALL-E 3	Firefly	FLUX	SD 3.5	Facebook	Reddit	Twitter	AUC↑/bAcc↑	
AUC / bAcc	RINE	ProGAN [43]	61.7 / 54.6	83.1 / 71.8	92.4 / 82.2	6.9 / 45.3	97.5 / 91.2	34.1 / 46.7	89.6 / 81.3	60.1 / 52.8	73.3 / 67.7	62.7 / 56.0	66.1 / 65.0
	"	LDM [10]	97.5 / 91.6	99.6 / 97.0	95.3 / 83.5	28.9 / 49.1	86.1 / 68.5	86.2 / 71.4	96.2 / 86.8	75.1 / 64.4	81.9 / 76.5	82.8 / 68.6	83.0 / 75.7
	"	Ours	99.5 / 93.8	99.9 / 94.1	95.8 / 89.1	87.0 / 79.0	96.5 / 89.7	91.7 / 85.4	89.6 / 82.0	81.1 / 73.4	73.6 / 69.0	84.7 / 76.1	89.9 / 83.2
	SigLip 512	D ³ [3]	99.0 / 65.2	100. / 86.7	99.7 / 60.2	100. / 85.1	99.9 / 55.9	96.7 / 56.2	99.3 / 68.5	89.8 / 79.4	75.2 / 71.6	92.6 / 78.1	95.2 / 70.7
"	Ours	99.8 / 96.4	99.7 / 96.4	92.9 / 83.9	99.0 / 95.2	99.9 / 96.9	94.8 / 87.7	93.4 / 86.8	95.7 / 90.3	82.3 / 75.5	96.0 / 90.3	95.4 / 89.9	
		Midjourney	SDXL	DALL-E 2	DALL-E 3	Firefly	FLUX	SD 3.5	facebook	reddit	twitter	NLL↓/ECE↓	
NLL / ECE	RINE	ProGAN [43]	5.03 / .410	1.99 / .236	0.77 / .135	20.5 / .546	0.36 / .053	10.1 / .506	1.22 / .149	6.51 / .454	2.46 / .242	5.23 / .393	5.43 / .312
	"	LDM [10]	0.26 / .094	0.18 / .111	0.35 / .132	1.44 / .350	0.52 / .115	0.51 / .103	0.33 / .126	0.61 / .107	0.51 / .065	0.55 / .115	0.53 / .132
	"	Ours	0.23 / .141	0.22 / .147	0.31 / .090	0.46 / .055	0.30 / .092	0.38 / .059	0.42 / .053	0.50 / .073	0.56 / .134	0.47 / .045	0.39 / .089
	SigLip 512	D ³ [3]	1.54 / .343	0.40 / .140	1.51 / .384	0.42 / .161	1.42 / .414	2.50 / .431	1.36 / .311	0.85 / .191	1.30 / .214	0.77 / .199	1.21 / .279
"	Ours	0.09 / .039	0.10 / .036	0.44 / .099	0.13 / .023	0.08 / .042	0.34 / .065	0.40 / .077	0.28 / .067	0.70 / .155	0.27 / .054	0.28 / .066	

Table 7. Ablation study on the influence of the training data. We compare the performance of a SoTA method, RINE [21], by varying the training data: ProGAN, LDM and our dataset. Then we train our model, SigLip [49], on a publicly available dataset, D³ [3], that includes 4 generators from the Stable Diffusion family. Performance are presented in terms of AUC/Accuracy (top) and ECE/NLL (bottom).

UnivFD [31]. It exploits pre-trained CLIP features through linear probing. Fine-tuning is carried out on the same dataset of real and GAN-generated images as in [43].

DeFake [37]. Both images and their corresponding prompts are used and fed into the visual and textual encoders of CLIP. The extracted features are the input of a multilayer perceptron trained for binary detection.

DIRE [44]. It uses the reconstruction error of a generative model as the input of a ResNet-50. In fact, this error is expected to be lower for synthetic images than for real ones.

AntifakePrompt [8]. It relies on a visual question-answering (VQA) tool, InstructBLIP. The VQA is used with a fixed question, "Is this photo real?", and fine-tuned to provide accurate responses ("Yes" or "No") using a soft prompt tuning technique. Note that the method provides hard binary predictions hence only balanced Accuracy can be computed.

NPR [39]. In this case a ResNet-50 is fed using a residual image computed as the difference between the original image and its interpolated version. The idea is to exploit the artifacts related to the up-sampling process which is common in several generative models.

FatFormer [27]. It adopts CLIP and introduces forgery-aware adapters to extract forensic traces from both space and frequency domains. The method proposes a language-guided alignment mechanism to supervise the process and ensure the association between image and text.

FasterThanLies [22]. The method employs a Binary Neural Network for features extraction phase and a linear classifier for detection. Beyond the image, the model has two additional input channels: the Fast Fourier Transform magnitude and the Local Binary Pattern image. We report results using the unfrozen BNext-M backbone.

RINE [21]. It uses features extracted from the intermediate blocks of a CLIP encoder and an additional trainable mod-

ule to take into account the influence of each block on the final decision.

AIDE [45]. It leverages hybrid features extracted from a ConvNeXt-based Open CLIP model and a CNN which is fed with patches filtered to remove semantic content and exploit low-level artifacts.

LaDeDA [6]. It is a patch-based classifier that leverages local image features. The image is split into multiple patches, for each patch a prediction is computed and then averaged to obtain the image-level prediction.

C2P-CLIP [40]. It uses the Low-Rank Adaptation (LoRA) strategy to fine-tune the image encoder of CLIP. Moreover, it relies on a contrastive learning strategy based on category prompts.

CoDE [3]. CoDE trains a Vision Transformer using a contrastive loss similar to CLIP. However, while CLIP aims to learn features for text-image matching, CoDE aims at obtaining an embedding space where real and fake images are effectively separated. We report results using CoDE in combination with a the linear classifier.

10. Calibration Metrics

Here we provide some more details about the calibration metrics used in the paper. The binary Expected Calibration Error (ECE) is defined as:

$$ECE = \sum_{m=1}^M \frac{|B_m|}{N} |\text{prob}(B_m) - \text{pred}(B_m)| \quad (1)$$

where N is the number of samples of the test-set, M is the number of bins, and B_m is the set of samples whose predictions fall into the m -th bin, with $|B_m|$ its cardinality. $\text{prob}(B_m)$ and $\text{pred}(B_m)$ are the actual probability and the average predicted probability of the target class in that bin, respectively. In case of unbalanced test-set, we weigh the contribution of each sample in the average to re-balance the relevance between two classes. We used $M = 15$ bins.

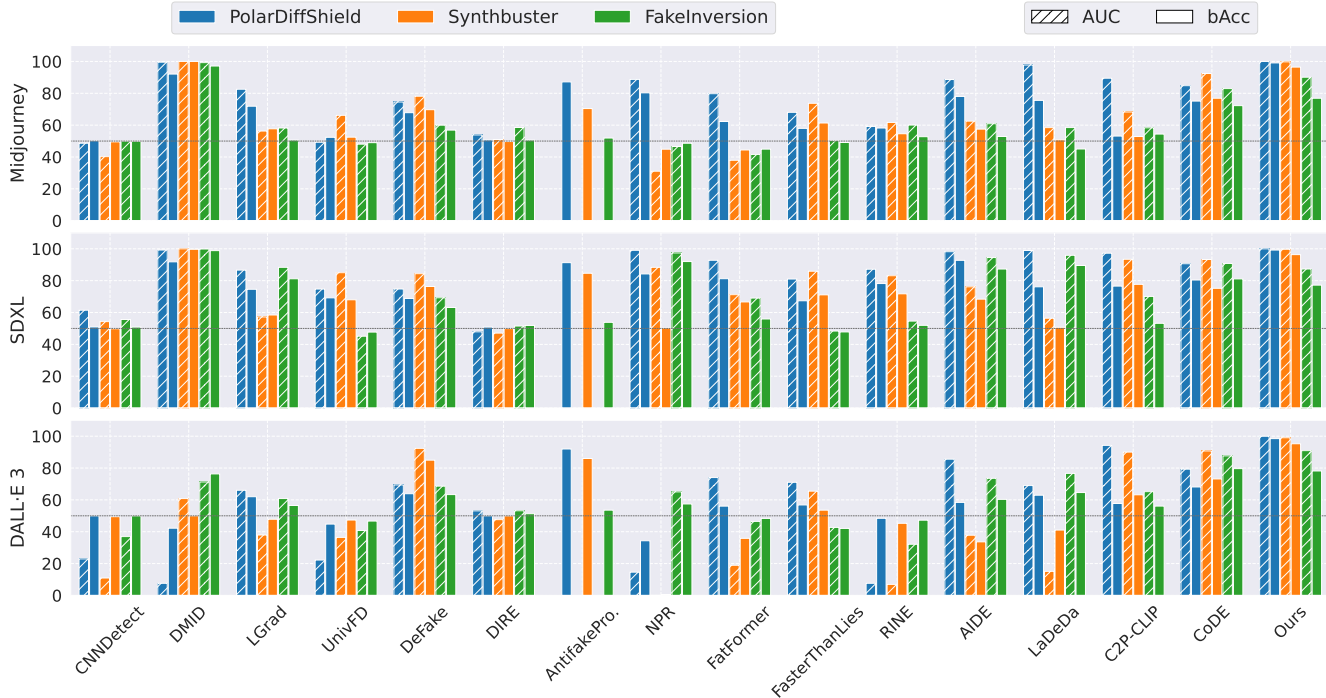


Figure 10. SoTA performance evaluated in terms of AUC and balanced Accuracy on Midjourney, SDXL and DALL-E generators from different datasets.

The balanced Negative Log-Likelihood (NLL) is defined as:

$$\text{NLL} = -\frac{0.5}{|S_0|} \sum_{i \in S_0} \log p_i(0) - \frac{0.5}{|S_1|} \sum_{i \in S_1} \log p_i(1) \quad (2)$$

where S_0 and S_1 are the set of samples of non-target and target class, respectively, while $p_i(0)$ and $p_i(1)$ are the predicted probabilities of the two classes for the i -th input sample.

11. Additional Ablation

In this Section we further investigate the influence of our training dataset. First of all, we consider a SoTA method, RINE [21], that is designed to exploit also low-level forensic features and compare different strategies. The model is trained on three different datasets: ProGAN [43], Latent Diffusion (LDM) [10] and the dataset with content augmentation we proposed in this work (*inpainted+*). Results are presented in Tab. 7 and show that our dataset is particularly helpful to obtain better and more calibrated results. On average we achieve an improvement of around 7% in terms of AUC and balanced accuracy compared to training on LDM, and a much larger gain, around 20% in terms of accuracy, with respect to ProGAN. The advantage seems to be significant especially for synthetic generators that are much different from Latent Diffusion, such as DALL-E 3, Firefly and FLUX.

We also conduct an additional experiment and train our network, SigLip [49], on the very recent Diffusion-generated Deepfake Detection (D^3) dataset [3], of about 8M synthetic images (from 256×256 to 1024×1024) from the generators SD 1.4, SD 2.1, SDXL, and DeepFloyd IF. The images are generated using prompts taken from the description of the real source from LAION (text-driven generation). We can notice that although the AUC is similar ($\approx 95\%$), there is a significant increase in terms of balanced accuracy (70.7 vs. 89.9) and decrease in terms of both NLL (1.21 vs 0.28) and ECE (0.28 vs 0.07). This confirms that our training paradigm enables better calibration and improved generalization.

12. Additional Generalization Analysis

In this Section we conduct further experiments which confirm that our method can generalize better than other methods and obtain less biased results. We also detail results and show the performance on each synthetic generator for GenImage and FakeBench datasets.

Evaluation on same generators from different datasets.

Here we further expand on the analysis conducted in Fig. 2 of the main paper where we have shown that some detectors achieve different performance on the same generator when the images are taken from two different datasets. This puzzling behavior suggests the possibility that these methods

AUC↑/bAcc↑	GenImage (unbiased)								
	BigGAN	VQDM	ADM	GLIDE	SD 1.4	SD 1.5	Midjourney	Wukong	AVG
CNNDetect	70.9 / 58.4	63.4 / 51.2	51.8 / 49.9	59.4 / 50.7	65.1 / 50.1	66.4 / 49.9	79.3 / 50.1	62.6 / 50.2	64.8 / 51.3
DMID	74.6 / 52.3	97.6 / 75.1	78.5 / 51.3	94.9 / 56.6	100. / 99.9	100. / 99.8	100. / 97.4	100. / 99.6	93.2 / 79.0
LGrad	18.7 / 28.9	23.9 / 30.8	24.6 / 30.5	22.2 / 30.0	50.0 / 49.8	49.2 / 49.1	50.5 / 50.6	47.6 / 46.9	35.8 / 39.6
UnivFD	96.7 / 86.1	94.8 / 79.7	85.2 / 64.4	88.8 / 63.9	78.7 / 55.5	78.1 / 56.6	74.0 / 54.2	86.9 / 63.7	85.4 / 65.5
DeFake	72.6 / 64.4	71.1 / 64.4	49.3 / 48.5	87.9 / 80.4	93.3 / 85.1	93.4 / 85.4	87.7 / 79.2	89.8 / 81.8	80.6 / 73.7
DIRE	26.6 / 46.9	35.0 / 47.7	25.3 / 46.7	29.9 / 47.0	41.7 / 47.3	39.8 / 47.3	38.0 / 47.5	45.4 / 47.7	35.2 / 47.3
AntifakePrompt	- / 81.7	- / 81.1	- / 81.6	- / 81.8	- / 77.1	- / 76.6	- / 70.4	- / 77.6	- / 78.5
NPR	56.9 / 56.3	52.3 / 53.9	46.9 / 50.5	42.1 / 48.3	54.3 / 49.4	53.3 / 49.7	42.3 / 47.4	52.4 / 50.2	50.1 / 50.7
FatFormer	88.5 / 80.1	84.5 / 71.5	69.1 / 60.4	78.4 / 65.1	49.8 / 52.0	48.7 / 53.3	46.2 / 51.6	61.6 / 58.1	65.9 / 61.5
FasterThanLies	78.9 / 54.1	86.8 / 76.6	88.6 / 77.2	83.0 / 66.1	97.8 / 92.2	97.9 / 92.3	83.1 / 69.7	95.4 / 88.1	88.9 / 77.0
RINE	99.4 / 88.5	98.4 / 81.4	93.8 / 63.9	98.1 / 74.7	93.9 / 60.5	94.1 / 61.1	86.3 / 52.4	95.7 / 70.0	95.0 / 69.1
AIDE	73.1 / 50.7	78.0 / 51.0	61.2 / 50.1	80.4 / 52.3	98.2 / 74.5	98.5 / 75.9	88.1 / 57.4	95.9 / 69.3	84.2 / 60.2
LaDeDa	93.1 / 80.3	10.8 / 34.8	6.8 / 34.6	8.8 / 34.5	55.6 / 54.8	53.6 / 53.0	51.3 / 52.1	61.6 / 57.7	42.7 / 50.2
C2P-CLIP	97.2 / 87.5	92.2 / 74.1	86.7 / 71.3	93.6 / 74.8	94.4 / 80.5	94.3 / 79.1	76.3 / 55.9	93.1 / 81.0	91.0 / 75.5
CoDE	70.2 / 50.0	66.8 / 56.0	53.7 / 51.9	78.1 / 58.0	99.4 / 96.6	99.2 / 96.5	86.0 / 69.6	99.1 / 95.0	81.6 / 71.7
Ours	98.6 / 94.6	96.9 / 90.8	97.1 / 92.7	92.9 / 83.3	98.9 / 93.5	98.7 / 93.5	95.8 / 89.0	99.1 / 94.1	97.3 / 91.4

Table 8. Performance on each generator included in GenImage (unbiased) dataset in terms of AUC and balanced Accuracy. Bold underlines the best performance for each column with a margin of 1%.

AUC↑/bAcc↑	FakeBench										
	ProGAN	StyleGAN	FuseDream	VQDM	GLIDE	CogView2	DALL-E 2	DALL-E 3	SD	Midjourney	AVG
CNNDetect	100. / 99.7	98.3 / 75.1	94.8 / 61.1	62.9 / 51.9	62.6 / 50.6	64.9 / 49.7	56.1 / 49.7	58.6 / 49.7	57.2 / 49.7	62.0 / 49.9	71.7 / 58.7
DMID	61.0 / 51.1	80.1 / 52.1	93.1 / 52.4	97.8 / 79.7	94.0 / 63.2	100. / 99.7	94.9 / 55.1	96.7 / 88.9	100. / 99.1	97.3 / 90.7	91.5 / 73.2
LGrad	96.8 / 77.1	82.3 / 72.9	18.9 / 28.4	75.2 / 68.6	41.8 / 43.9	23.7 / 33.6	10.9 / 27.6	30.6 / 35.6	24.7 / 34.1	76.1 / 67.3	48.1 / 48.9
UnivFD	99.9 / 98.6	96.0 / 83.4	99.2 / 96.3	94.6 / 77.3	86.5 / 62.8	84.7 / 63.1	88.0 / 65.9	69.6 / 55.8	76.8 / 56.4	65.5 / 55.6	86.1 / 71.5
DeFake	63.7 / 58.1	73.7 / 66.7	53.8 / 51.0	69.8 / 64.5	81.6 / 74.2	84.7 / 77.2	83.6 / 76.5	81.7 / 74.5	86.4 / 77.3	78.7 / 70.5	75.8 / 69.0
DIRE	90.4 / 89.5	56.6 / 55.4	23.7 / 40.0	91.3 / 89.2	53.2 / 63.7	36.7 / 41.0	44.2 / 43.0	76.6 / 74.5	47.7 / 49.7	83.4 / 81.2	60.4 / 62.7
AntifakePrompt	- / 79.0	- / 78.0	- / 78.6	- / 77.0	- / 78.8	- / 75.8	- / 73.4	- / 74.0	- / 71.6	- / 76.1	- / 76.2
NPR	99.5 / 92.4	78.1 / 68.1	48.7 / 42.7	93.4 / 90.9	67.0 / 65.2	50.3 / 42.7	41.7 / 42.9	46.3 / 44.6	57.5 / 51.4	89.0 / 84.6	67.1 / 62.5
FatFormer	100. / 97.6	99.3 / 97.1	90.7 / 81.8	96.8 / 88.5	74.2 / 69.0	47.1 / 53.3	45.3 / 48.1	52.4 / 49.5	50.4 / 51.0	79.6 / 64.6	73.6 / 70.0
FasterThanLies	87.0 / 80.2	72.4 / 57.7	85.7 / 75.4	54.7 / 45.9	76.9 / 62.5	96.0 / 87.7	92.9 / 85.7	73.6 / 60.6	93.6 / 84.5	67.6 / 57.7	80.0 / 69.8
RINE	100. / 99.6	99.3 / 95.1	99.8 / 96.6	98.8 / 88.6	95.4 / 70.2	86.7 / 59.2	93.0 / 60.9	75.1 / 52.6	85.5 / 55.9	82.2 / 61.1	91.6 / 74.0
AIDE	89.4 / 64.3	89.4 / 70.0	71.7 / 47.3	90.7 / 78.1	79.7 / 68.3	85.5 / 60.0	84.1 / 52.6	88.0 / 61.9	86.0 / 64.6	88.0 / 71.5	85.2 / 63.9
LaDeDa	98.0 / 82.5	94.5 / 82.5	37.2 / 40.5	85.8 / 81.5	52.6 / 57.3	39.4 / 41.6	36.4 / 35.3	49.9 / 45.1	45.3 / 46.1	90.7 / 78.1	63.0 / 59.1
C2P-CLIP	100. / 99.5	99.4 / 98.0	98.2 / 93.0	97.1 / 86.7	91.9 / 76.4	67.3 / 61.7	72.6 / 56.9	74.7 / 55.5	74.9 / 59.9	88.1 / 58.0	86.4 / 74.6
CoDE	64.3 / 52.5	53.0 / 49.5	73.4 / 56.3	78.4 / 61.7	91.6 / 78.0	97.7 / 93.7	93.8 / 82.8	95.8 / 89.2	99.5 / 96.2	89.7 / 76.7	83.7 / 73.7
Ours	94.7 / 88.3	93.6 / 88.1	90.3 / 80.5	95.3 / 89.3	89.4 / 79.1	95.4 / 88.1	91.6 / 83.2	97.1 / 91.5	95.4 / 88.5	96.3 / 90.1	93.9 / 86.7

Table 9. Performance on each generator included in FakeBench dataset in terms of AUC and balanced Accuracy.

rely on subtle dataset biases besides true traces left by the synthetic generator. In Fig. 10 we extend this analysis to all SoTA methods described in Sec. 9. More specifically, we analyze the performance in terms of AUC and balanced accuracy over three synthetic generators: Midjourney, SDXL and DALL-E 3 that come from three different datasets PolarDiffShield [23], Synthbuster [2] and FakeInversion [7]. As said before, for several methods the performance is not consistent on the same generator and can vary even by 20% from one dataset to another. In addition, for some methods the AUC is around 50%, which corresponds to random choice, or even below 50% which means that the detector tends to invert the labels between real and fake.

Evaluation on different synthetic generators. We conduct a more detailed analysis of the results on GenImage (unbiased), where fake images have been subjected to JPEG compression, similar to real images, to prevent detectors

from exploiting compression artifacts. We also consider FakeBench [24], that consists of 3,000 real and 3,000 fake images generated by 10 different models. These datasets include both GAN and Diffusion-based synthetic images, which allows us to better understand the ability of our approach to generalize to different architectures. Results are presented in Tab. 8 and Tab. 9. We note that our approach obtains very good results consistently across almost all generators, while other methods, such as DMID, UnivFD, RINE, FasterThanLies, and FatFormer, perform very well in terms of AUC only on certain generators. In addition, for our method the gap between AUC and balanced accuracy is reduced which ensures more reliable results.

13. Additional Robustness Analysis

Here we want to further investigate the performance of our method compared to SOTA in terms of robustness. To this

	Original		Social network simulation	
	AUC↑/bAcc↑	NLL↓/ECE↓	AUC↑/bAcc↑	NLL↓/ECE↓
CNNDetect	54.3 / 50.9	7.94 / .488	51.8 / 50.1	8.73 / .498
DMID	97.3 / 96.1	0.25 / .041	94.3 / 81.3	0.55 / .182
LGrad	84.3 / 77.2	2.27 / .200	60.1 / 55.4	7.59 / .426
UnivFD	54.9 / 52.8	2.19 / .391	49.7 / 49.9	2.57 / .434
DeFake	69.8 / 63.3	0.95 / .225	69.3 / 62.6	0.98 / .236
DIRE	53.3 / 51.8	13.4 / .360	55.4 / 51.6	13.4 / .358
AntifakePrompt	- / 53.9	- / -	- / 54.7	- / -
NPR	91.5 / 87.0	4.96 / .123	43.3 / 49.9	27.1 / .501
FatFormer	68.1 / 59.7	3.45 / .386	48.6 / 50.3	5.44 / .490
FasterThanLies	49.7 / 48.6	3.64 / .476	50.9 / 49.9	3.13 / .458
RINE	69.6 / 63.6	4.84 / .319	62.3 / 52.9	6.28 / .437
AIDE	85.5 / 76.9	0.54 / .137	67.2 / 56.3	0.93 / .276
LaDeDa	91.6 / 84.7	3.03 / .129	51.9 / 53.1	24.8 / .454
C2P-CLIP	74.1 / 59.6	0.82 / .260	71.8 / 59.0	0.89 / .284
CoDE	87.5 / 78.7	0.74 / .143	82.5 / 74.4	0.89 / .171
Ours (inpainted+)	94.0 / 79.6	0.76 / .182	89.3 / 77.3	0.80 / .176
Ours (inpainted++)	95.8 / 82.0	0.44 / .154	93.7 / 82.5	0.42 / .122

Table 10. Performance on FakeInversion dataset. We show results on the original dataset and on a post-processed version, to simulate the upload on social networks.

end, we analyze two variants of our method, content augmentation and diverse category (*inpainted+*) and with additional standard augmentation operations (*inpainted++*).

Analysis of post-processing operations. We show further results on FakeInversion [7], where the real images have been retrieved from the web. To better understand the effect of compression and resizing we compare the performance when applying such operations. In particular, to simulate the upload on social networks, we resize with a scale factor randomly sampled between 0.7 and 1, and compress with a JPEG quality factor between 70 and 100. In Tab. 10 results show that the performance on such dataset drops substantially, except for DMID and our method, though our approach *inpainted++* has slightly better calibration metrics.

Analysis on content shared on-line. Fig. 11 illustrates the balanced accuracy on real/fake images shared on the web,

with multiple versions of the same image (as already shown for the proposal in Fig. 7 of the main paper). Accuracy is evaluated over a 100-day period from the time of initial publication of each image, with times on a logarithmic scale. We compare our proposal with the best performing SoTA methods on this dataset of around 1400 images. We can notice that the performance drops after only one day, after which most competitors are stuck below 65%. Only the variant *inpainted++* of the proposed method that comprises more aggressive augmentation is able to ensure an average accuracy around 85% even after many days from the first on-line post.

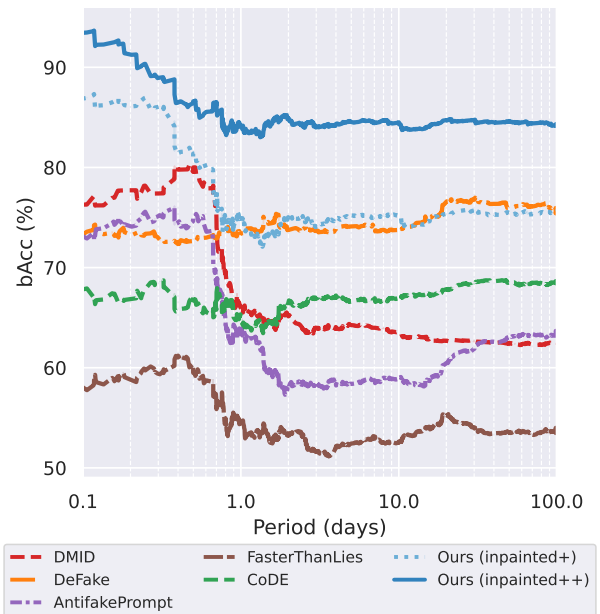


Figure 11. Results of SoTA detectors on real and fake images that went viral on internet. The performance is in term of balanced accuracy evaluated from the initial online post (Log scale).